A comparison between numerical and approximate methods for rapid calculation of NSIFs

Marcello Lepore[a,*], Klas Solberg[b], Filippo Berto[b]

[a] Department of Industrial Engineering, University of Salerno, Via G. Paolo II 132, 84084 Fisciano (SA), Italy
[b] Department of Mechanical and Industrial Engineering, NTNU, Richard Birkelands vei 2b, 7491 Trondheim, Norway

ABSTRACT

To more rapidly predicting the integrity of components weakened by sharp notches, notch stress intensity factors (NSIFs) are usually evaluated. Many methods have been proposed evaluating NSIFs, ranging from the stress gradient based formulation to methods evaluating strain energy density averaged over a control region. Here, we compare different numerical and approximate methods applied to a square plate with a 45° tilted crack, positioned at the center of the plate. Hence, approximate methods need to FE solutions, obtained from models discretized with fine mesh or, alternatively, with coarse mesh, having to consider the mean value of the local Strain Energy Density (SED) to calculate NSIFs. Furthermore, 2D and 3D numerical simulations have been carried out to investigate the solutions provided by these analytical methods. For this aim, two software based on the Finite Element Method (FEM) and on the Dual Boundary Element Method (DBEM), respectively, have been adopted to solve the proposed study case of the square plate with a 45° tilted crack. These methods can supply accurate predictions of SIFs by means of J-integral calculation. Then, the NSIFs have been calculated at the intersection between the crack front and the free surface of the plate and, to assess the thickness effect on the provided solutions, they have also been calculated at half the thickness along the crack front and for increasing thickness values. Finally, the NSIFs obtained from the analytical and numerical methods have been compared each other to evaluate the level of agreement.

1. Introduction

NSIFs play an essential role in static strength assessments of components made of brittle or quasi-brittle materials, weakened by sharp notches [1]. This holds true also for components made of structural materials undergoing high cycle fatigue loading [2] as well as for welded joints [3,4]. In recent years, some approximate methods based on the evaluation of the Averaged Strain Energy Density (ASED) were proposed. One of the first and most significant models available in the Literature was proposed by Lazzarin et al., based on the calculation of the Strain Energy Density (SED) averaged in two different control volumes centered at the notch tip [5,6]. More recently, another approximate method has been presented by Treifi and Oyadiji that takes advantage of the strain energy density averaged within two control volumes (semi-circular sector) centered at the notch tip [7]. Furthermore, a new method based on the evaluation of the total and deviatoric strain energy density averaged over a control volume was proposed [8,27]. The new method and a modified version were compared to the methods of Lazzarin et al. and Treifi and Oyadiji showing higher accuracy [27]. A comparison between different failure criteria for V-shaped notches has been done by Lazzarin et al. [29]. The finite fracture mechanics criteria by Leguillon [30] and Carpinteri [31] were compared to SED, both analytically and by use of finite element for calculating NSIF. All the methods gave good agreement with experiment results.

In this work, the SED based methods described above were applied to a square plate weakened by a 45° tilted crack positioned at the center of the plate. When the opening angle of a v-shaped notch being zero, the v-notch turns into a crack. Hence, NSIFs are firstly calculated according to the Gross and Mendelson equations [9], by means of FE refined mesh, and then approximate methods with coarse mesh were used to calculate NSIFs by means of the ASED. Furthermore, two numerical analyses of the notched plate were performed using the Dual Boundary Element Method (DBEM) both considering 2D and 3D cases. After that, a numerical analysis was carried out with a FEM-based software for the one 3D case. The normalised SIFs, obtained by the overall numerical investigations, were compared with each other and with normalised SIFs obtained from the approximate methods. The

* Corresponding author.
E-mail address: malepore@unisa.it (M. Lepore).

Nomenclature

ASED	averaged strain energy density
a	crack length
C_a, C_b	constants of $W_{a,FE}$ and $W_{b,FE}$
DBEM	dual boundary element method
DSED	deviatoric strain energy density
D_a, D_b	constants of $W_{a,FE}$ and $W_{b,FE}$
E	Young's modulus
ERR	energy release rate
FEM	finite element method
I_1, I_2	integrals of the angular stress functions
J	J-integral
K_I, K_{II}	mode I, II stress intensity factors
K_1, K_2	normalised mode I, II of stress intensity factors
LB	large Block
LEFM	Linear Elastic Fracture Mechanics
NSIF	Notch Stress Intensity Factor
R	control radius
R_a, R_b	outer and inner control radii
R_0	radius of the control volume
SB	standard Block
SED	Strain Energy density
SIF	Stress Intensity Factors
W_a,FE	SED component
W_b,FE	SED component
r, θ	polar system coordinates
t	thickness of the plate
2α	notch opening angle
γ	notch bisector angle
υ	Poisson's ratio
λ_1, λ_2	mode I, II first eigenvalues in William's equations
$\sigma_{\theta\theta}$, $\tau_{r\theta}$	notch tip stress components
Ω	volume control

thickness effect on normalised SIFs was inferred by means of three-dimensional FE analyses, varying the thickness from 1.0 mm up to 3.0 mm on the same geometrical model.

2. Methods

2.1. Model geometry, boundary and loading conditions

The special case of a square plate weakened by a 45 tilted crack is studied. The geometry is shown in Fig. 1, the notched square plate subjected to mixed mode I + II loading. The geometry of the plate is characterized by equal width and height, $2W = H = 10$ mm. The tilted crack in the plate of finite extension (Fig. 6) can be described by a projected crack length $2a = 2$ mm and a crack inclination angle $\phi = 45^{\circ}$. For the numerical calculations, FEM and DBEM simulations were employed to model the plate and obtain SIFs. The boundary conditions and loads are shown in Fig. 1b.

2.2. Background

In plane problems, the mode I and mode II NSIFs for sharp V-notches, which quantify the intensity of the asymptotic stress distributions in the close neighborhood of the notch tip, is expressed by means of the Gross and Mendelson's [9] equations:

$$K_1 = \sqrt{2\pi}\lim_{r\to 0}[(\sigma_{\theta\theta})_{\theta=0} * r^{(1-\lambda_1)}] \tag{1}$$

$$K_2 = \sqrt{2\pi}\lim_{r\to 0}[(\tau_{r\theta})_{\theta=0} * r^{(1-\lambda_2)}] \tag{2}$$

where (r, θ) are the component of the polar coordinate system centered at the notch tip (Fig. 1), $\sigma_{\theta\theta}$ and $\tau_{r\theta}$ are the stress components according to the coordinate system; λ_1 and λ_2 are respectively the mode I and mode II first eigenvalues in William's equations [10]. The main practical disadvantage in the application of the NSIF-based approach is that very refined meshes are needed to calculate the NSIFs by means of Eqs. (1) and (2). Refined meshes are not necessary when the aim of the finite element analysis is to assess the mean value of the local strain energy density on a control volume surrounding the stress singularity. In fact, SED can be derived directly from nodal displacements, so that also coarse meshes are able to give accurate values. Recently, some approximate methods for the rapid calculation of the NSIFs, based on the averaged strain energy density (ASED) have been proposed [5]. The total elastic strain energy density averaged over a sector of radius R_0 has been widely used in the Literature also for static [11–15] and fatigue strength assessments [6,16]. In the case of mixed mode loading, these methods require the solution of a system of two equations in two unknowns (K_1 and K_2). Furthermore, a method based on the evaluation of the total and deviatoric SED (DSED), averaged in a single control volume, has been considered. Also, in this case, two independent equations can be obtained, one linked to the total SED and the other to the deviatoric one: in this way it is possible to evaluate the SIFs, K_I and K_{II}, of cracks under mixed mode loading (see Fig. 2).

2.3. Approximate methods

2.3.1. Lazzarin et al. approach

This method has been proposed by Lazzarin et al. [4] and it is based on the evaluation of the ASED on two different control volumes (circular sectors), centered at the notch tip and characterized by the radii R_a and R_b (Fig. 3a). Known the SED values (W_a and W_b), by means of a FE analysis, and defined the control radii (R_a and R_a), it is possible to obtain a system of two equations in two unknowns (K_1 and K_2):

$$\begin{cases} W_{a,FE} = \frac{1}{2E}\left[\frac{I_1}{2\lambda_1\gamma} * \frac{K_1^2}{R_a^{2(1-\lambda_1)}} + \frac{I_2}{2\lambda_2\gamma} * \frac{K_2^2}{R_a^{2(1-\lambda_2)}}\right] = C_a * K_1^2 + D_a * K_2^2 \\ W_{b,FE} = \frac{1}{2E}\left[\frac{I_1}{2\lambda_1\gamma} * \frac{K_1^2}{R_b^{2(1-\lambda_1)}} + \frac{I_2}{2\lambda_2\gamma} * \frac{K_2^2}{R_b^{2(1-\lambda_2)}}\right] = C_b * K_1^2 + D_b * K_2^2 \end{cases} \tag{3}$$

where E is the Young's modulus of the material whilst I_1 and I_2 are the integrals of the angular stress functions, which depend on the notch opening angle, $2\alpha = 2\pi - 2\gamma$, and the Poisson's ratio ν. This method cannot be applied to a crack subjected to mixed mode loading, since an indeterminate system of equations would be obtained. Solving the system of equations, the values of the NSIFs can be determined as follows:

$$K_1 = \sqrt{\frac{D_a * W_{b,FE} - D_b * W_{a,FE}}{D_a * C_b - D_b * C_a}} \tag{4}$$

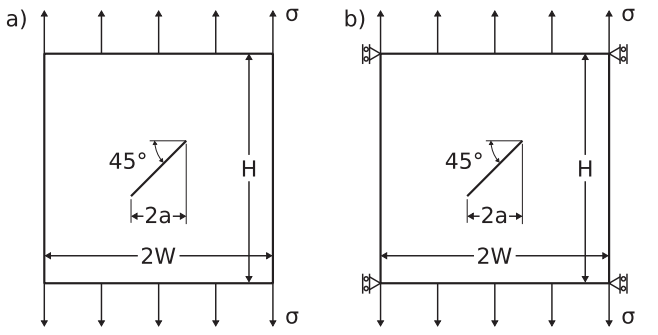

Fig. 1. Loaded square plate with the 45° tilted crack (a) and loads and boundary conditions applied in FEA (b).

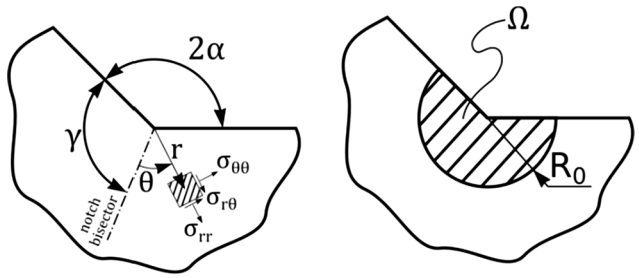

Fig. 2. Polar coordinate system centered at the notch tip [27].

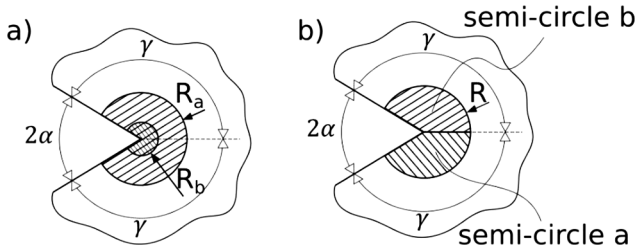

Fig. 3. Control volumes in the Lazzarin et al. approach (a) and in the Treifi and Oyadiji approach (b) [27].

$$K_2 = \sqrt{\frac{W_{a,FE} - C_a * K_1^2}{D_a}} \tag{5}$$

2.3.2. Treifi and Oyadiji approach

The method has been proposed by Treifi and Oyadiji [7] and it is based on the evaluation of the averaged SED on two different control volumes (semi-circular sectors with a central angle equal to γ) centered at the notch tip and characterized by a radius R (Fig. 3b). Known the SED values (W_a and W_b) by means of a FE analysis, and defined the control radius (R), it is possible to obtain a system of two equations in two unknowns (K_1 and K_2):

$$\begin{cases} W_{a,FE} = \frac{1}{2E}\left[\frac{I_{1,s}}{\lambda_1\gamma} * \frac{K_1^2}{R^{2(1-\lambda_1)}} + \frac{I_{2,s}}{\lambda_2\gamma} * \frac{K_2^2}{R^{2(1-\lambda_2)}} + \frac{2*I_{12,s}}{(\lambda_1+\lambda_2)\gamma} * \frac{K_1K_2}{R^{2-\lambda_1-\lambda_2}}\right] = \\ = M * K_1^2 + N * K_2^2 + Q * K_1 * K_2 \\ W_{b,FE} = \frac{1}{2E}\left[\frac{I_{1,s}}{\lambda_1\gamma} * \frac{K_1^2}{R^{2(1-\lambda_1)}} + \frac{I_{2,s}}{\lambda_2\gamma} * \frac{K_2^2}{R^{2(1-\lambda_2)}} - \frac{2*I_{12,s}}{(\lambda_1+\lambda_2)\gamma} * \frac{K_1K_2}{R^{2-\lambda_1-\lambda_2}}\right] = \\ = M * K_1^2 + N * K_2^2 - Q * K_1 * K_2 \end{cases} \tag{6}$$

where $I_{1,s}$, $I_{2,s}$ and $I_{12,s}$ are the integrals of the angular stress functions, which depend on the notch opening angle, 2α, the angle defined by the semi-circular sector, γ, and the Poisson's ratio ν. In this case the contribution of the mixed term ($K_1 \cdots K_2$) is present because the integration for the strain energy evaluation is not performed on a control volume symmetrical with respect to the notch bisector line (Fig. 3b). Due to the presence of the mixed term, it is possible to decouple the contributions of the loading modes, obtaining a solution of the system even in the crack case. Solving the system of equations, the values of the NSIFs can be determined:

$$K_1 = \sqrt{\frac{(W_{a,FE} + W_{b,FE}) \pm \sqrt{(W_{a,FE} + W_{b,FE})^2 - \frac{4*M*N*(W_{a,FE}+W_{b,FE})^2}{Q^2}}}{4 * M}} \tag{7}$$

$$K_2 = \frac{W_{a,FE} - W_{b,FE}}{2 * Q * K_1} \tag{8}$$

2.3.3. Approach based on the deviatoric SED

This approach has been presented for the first time in Ref. [5]. It is based on the evaluation of the total and deviatoric SED averaged in a single control volume (circular sector) centered at the notch tip and characterized by a radius R (Fig. 4a). Two independent equations can be obtained: one linked to the total SED and the other to the deviatoric one. In this way, it is possible to obtain a solution of the system even in the crack case.

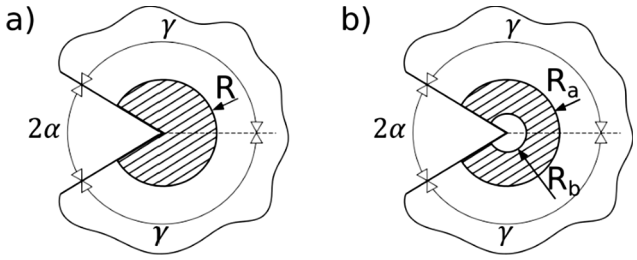

Fig. 4. Control volumes in the approach based on the deviatoric SED (a) and in the modified version of the approach based on the deviatoric SED (b) [27].

As previously, knowing the SED values (W and W_{dev}), by means of a FE analysis, and defining the control radius (R), it is possible to obtain a system of two equations in two unknowns (K_1 and K_2):

$$\begin{cases} W_{FE} = \frac{1}{2E}\left[\frac{I_1}{2\lambda_1\gamma} * \frac{K_1^2}{R^{2(1-\lambda_1)}} + \frac{I_2}{2\lambda_2\gamma} * \frac{K_2^2}{R^{2(1-\lambda_2)}}\right] = S * K_1^2 + T * K_2^2 \\ W_{dev,FE} = \frac{1+\upsilon}{3E}\left[\frac{I_{1,dev}}{2\lambda_1\gamma} * \frac{K_1^2}{R^{2(1-\lambda_1)}} + \frac{I_{2,dev}}{2\lambda_2\gamma} * \frac{K_2^2}{R^{2(1-\lambda_2)}}\right] = S_{dev} * K_1^2 + T_{dev} * K_2^2 \end{cases} \tag{9}$$

where $I_{1,dev}$ and $I_{2,dev}$ are the integrals of the angular stress functions related to the deviatoric strain energy density, which depend on the notch opening angle, 2α, and the Poisson's ratio ν. Solving the system of equations, the values of the NSIFs can be determined:

$$K_1 = \sqrt{\frac{T * W_{dev,FE} - T * W_{FE}}{T * S_{dev} - T_{dev} * S}} \tag{10}$$

$$K_2 = \sqrt{\frac{W_{dev,FE} - S_{dev} * K_1^2}{T_{dev}}} \tag{11}$$

As discussed earlier, the total SED can be derived directly from nodal displacements, so that also coarse meshes are able to give accurate values for it. However, the calculation of the deviatoric SED, by a FE code, is based on the von Mises equivalent stress averaged within the element. This quantity is more sensitive to the refinement level of the adopted mesh, so that the new proposed method could not be mesh-insensitive. With the aim to improve the results obtained from the application of the new method (based on the deviatoric SED) in the case of coarse meshes, a modified version has been proposed. This approach is similar to the previous one, but it is applied to a control volume consisting of a circular ring (Fig. 4a). The calculation of the deviatoric SED, by a FE code, is based on the von Mises equivalent stress averaged within the element that is a parameter sensitive to the refinement level of the adopted mesh. In case of coarse meshes it could be useful to exclude from the calculation the area characterized by the highest stress gradient (i.e. the region close to the notch tip). The control volume results to be constituted by a circular ring characterized by an outer radius R_a and by an inner radius R_b (Fig. 4b). As before, knowing the SED values (W and W_{dev}), by means of a FE analysis, and defining the control radii (R_a and R_b), it is possible to obtain a system of two equations in two unknowns (K_1 and K_2):

$$\begin{cases} W_{FE} = \frac{1}{2E\gamma(R_a^2 - R_b^2)}\left[\frac{I_1 * K_1^2}{2\lambda_1} * \left(\frac{1}{R_a^{-2\lambda_1}} - \frac{1}{R_b^{-2\lambda_1}}\right) + \frac{I_2 * K_2^2}{2\lambda_2} * \left(\frac{1}{R_a^{-2\lambda_2}} - \frac{1}{R_b^{-2\lambda_2}}\right)\right] \\ W_{dev,FE} = \frac{1+\upsilon}{3E\gamma(R_a^2 - R_b^2)}\left[\frac{I_{1,dev} * K_1^2}{2\lambda_1} * \left(\frac{1}{R_a^{-2\lambda_1}} - \frac{1}{R_b^{-2\lambda_1}}\right)\right. \\ \qquad \left. + \frac{I_{2,dev} * K_2^2}{2\lambda_2} * \left(\frac{1}{R_a^{-2\lambda_2}} - \frac{1}{R_b^{-2\lambda_2}}\right)\right] \end{cases} \tag{12}$$

Solving this system of equations, as already shown in the previous cases, the values of the NSIFs can be determined.

2.3.4. SIFs normalization

Methods described in Section 2 have been applied to the case of study of a notched plate subjected to mixed mode I + II loading. Normalised SIFs, K_1 and K_2, are calculated according to the Gross and Mendelson Eqs. (1) and (2), by means of several FE analyses and adopting very refined meshes in the close neighborhood of the notch tip (the size of the smallest element is of the order of 10^{-5} mm). Afterwards, the approximate methods have been applied taking into consideration three different values of the control radius R_0 (0.1, 0.01 and 0.001 mm) and by using of a coarse FE meshes. Hence, the FE mesh has been made of 8-node elements (PLANE 183) generated by means of the FE code ANSYS® 14.5. In the FE analyses, a Poisson's ratio ν equal to 0.3 and a Young's modulus E equal to 206 GPa have been adopted. The NSIFs have been reported in Table 1, according to the following definition:

$$K_{i,normalized} = \frac{K_i}{\sigma * \sqrt{\pi} * a^{1-\lambda_i}} \tag{13}$$

2.3.5. Numerical methods to calculate NSIFs

For the previous case of study of the notched plate, the 2D and 3D numerical analyses have been performed using FEM and DBEM approaches, respectively, and to compare the NSIFs calculated by different methods. Thus, the NSIFs have been computed where the crack front intersecting the free surface of the plate. In addition, using the DBEM-based approach (Beasy), the same problem for the 2D and 3D analyses has been solved while, using FEM-based approach (Abaqus and Zencrack software) only 3D analysis has been solved because Zencrack has the limit of only work in a 3D environment." Then, the stress scenario obtained from the several simulations has been compared. A similar comparison of the normalised SIFs, calculated at different distances from the crack front, has been carried out. Furthermore, the FEM-based analysis has been solved considering both standard (SB) and large (LB) cracked blocks to model the crack front with different j-path radii. Then, if SBs have been employed, the j-path radius is equal to 0.002 mm whilst, if LBs have been employed, the j-path radius is equal to 0.1 mm (Table 2). For the DBEM-based analyses, two j-path radii have been considered, that is, R = 0.07 for the 2D case and R = 0.1 for the 3D case, respectively.

2.3.6. Methods for calculating fracture parameters

Zencrack [17] is a fracture mechanics tool designed to interact with FEM-based software like Ansys or Abaqus [18]. By means of a Graphic User Interface (GUI), Zencrack allows to easily insert a single crack or multiple cracks through the substitution of hexahedral elements of the uncracked model, that contain a part of the crack front, with hexahedral elements belonging to special crack blocks for modelling the crack front [17]. Moreover, this substitution implies an adaptation of the surrounding mesh through a controlled and gradual deformation of neighboring elements carried out by means of a remeshing algorithm. It is worth noting that crack modelling is only possible if the mesh of the uncracked starting model is made of hexahedral elements [17]. In this work, the interaction between Zencrack and Abaqus allows inserting the crack in the uncracked model and simulating the behaviour of the cracked model under the action of the tensile load. Furthermore, Zencrack allows processing fracture parameters carried out from the FE simulation directly in the GUI.

Each crack is modelled by means of a set of collapsed blocks that are distinct in two groups: the first, consisting of collapsed facing elements used for modelling the crack front; the second, consisting of a pair of facing blocks whose adjacent nodes are separated each other to model the crack faces. Each cracked block is a set of 3D elements positioned inside a cube to hold each part of the crack front; each crack face has been modelled with only one block or multiple adjacent blocks depending on the crack extension. Moreover, each cracked block is stored in a Zencrack library in the form of families. In the cracked blocks library, two macro families of collapsed blocks are distinct: the first, containing "standard" blocks; the second, containing the "large" blocks. The FE simulations shown in this work use "standard" and "large" blocks, respectively. Zencrack calculates the Energy Release Rate (ERR) for each node of the crack front by the corresponding value of the J-Integral provided from Abaqus.

2.3.7. FE analysis using collapsed standard blocks

Using the SBs family SB04 [17] is useful to generate J-paths with a small radius for J-integral calculation. Generally, using SBs needs a bigger computational time for crack insertion and crack solution than the needed of LBs. In this study, the choice of the best approach depends essentially by the model and crack geometry. Fig. 5 shows the FE model of a square plate with highlight of the strategy used to model the central area where an inclined 45° crack will take place. Abaqus tie constraints are not employed in this case, then the model geometry is continuous everywhere as well as the mesh generated to discretize the model.

2.3.8. FE analysis using collapsed large blocks

The use of LBs imposes to model the square plate geometry with two distinct solid parts, as shown in Fig. 5. The adopted strategy of modelling introduces a discontinuity in the body geometry that is between the external surfaces of the Part 2, where the 45° tilted crack will take place, and the internal surface of the Part 1 (Fig. 6). Thus, also the mesh adopted to discretize these two parts will be discontinuous at the interface between the two parts. However, Abaqus allows introducing "tie constraints" conditions on the interfaces between the two parts that solves the problem of the mesh discontinuity [18]. Furthermore, because the Part 1 is defined as master whilst the Part 2 is defined as slave, the Part 2 should be discretized with a finer mesh than the Part 1. In general, the nodes on interface of each part will not coincident each other, thus the results in terms of nodal displacements and nodal stresses will be inaccurate. Refining the mesh on these interfaces could be a good modelling strategy to solve this problem; in this way, the interpolated values of nodal stresses and nodal displacements will

Table 1
Comparison between approximate methods for NSIFs evaluation of central tilted crack (2α = 0°) in a plate of finite extension [27].

		Coarse mesh (64 finite elements)			
R_0 [mm]	Method	K_1	K_2	ΔK_1 (%)	ΔK_2 (%)
	Gross and Mendelson	0.655	0.638		
0.1	Treifi and Oyadiji	0.636	0.642	−2.90	0.63
0.1	Method based on DSED	0.697	0.620	6.41	−2.82
0.1	DSED modified method	0.639	0.645	−2.44	1.10
0.01	Treifi and Oyadiji	0.613	0.654	−6.41	2.51
0.01	Method based on DSED	0.708	0.616	8.09	−3.45
0.01	DSED modified method	0.653	0.640	−0.31	0.31
0.001	Treifi and Oyadiji	0.624	0.651	−4.73	2.04
0.001	Method based on DSED	0.712	0.615	8.70	−3.61
0.001	DSED modified method	0.657	0.639	0.31	0.16

Table 2
Comparison between the K_1 and K_2 calculated with the approximate methods for NSIFs evaluation and the corresponding calculated by 2D and 3D numerical analyses by DBEM (red) and FEM (green) approaches.

		Coarse mesh (64 finite elements)				*Refined mesh (3395 finite elements)*			
R_0 [mm]	*Method*	K_1	K_2	ΔK_1 (%)	ΔK_2 (%)	K_1	K_2	ΔK_1 (%)	ΔK_2 (%)
	Gross and Mendelson	0.655	0.638						
0.1	Treifi et al.	0.636	0.642	-2.90	0.63	0.660	0.637	0.76	0.16
0.1	Method based on DSED	0.697	0.620	6.41	-2.82	0.639	0.645	2.44	1.10
0.1	DSED modified method	0.639	0.645	-2.44	1.10				
0.1	FEM LB06					0.646	0.794	0	0
0.07	DBEM 2D					0.654	0.639	0	0
0.1	FEM LB02					0.642	0.798	0	0
0.1	DBEM 3D					0.608	0.779	0	0
0.01	Treifi et al.	0.613	0.654	-6.41	2.51	0.635	0.647	3.05	1.41
0.01	Method based on DSED	0.708	0.616	8.09	-3.45	0.653	0.640	0.31	0.31
0.01	DSED modified method	0.653	0.640	-0.31	0.31				
0.002	FEM SB04					0.610	0.754	0	0
0.001	Treifi et al.	0.624	0.651	-4.73	2.04	0.644	0.644	-1.68	0.94
0.001	Method based on DSED	0.712	0.615	8.70	-3.61	0.662	0.636	1.07	-0.31
0.001	DSED modified method	0.657	0.639	0.31	0.16				

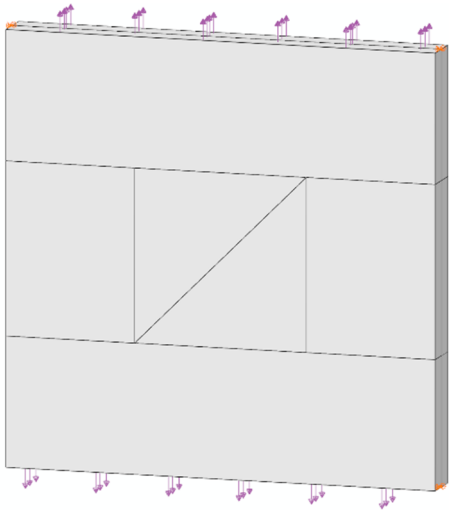

Fig. 5. Assembly of the square plate with highlight of the adopted geometry and boundary conditions.

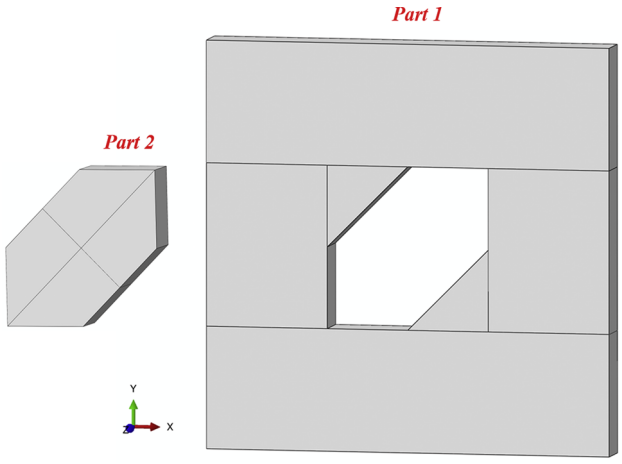

Fig. 6. Highlighting of the Part 1 and Part 2 of the assembly. Tie constraint conditions have been applied at interfaces between the two parts.

describe accurately the respective fields of stress and displacement, producing a solution that correctly predicts the behavior of the loaded plate. Furthermore, the use of LBs is very useful when it is needed to propagate a crack, because it is avoided an undesirable and excessive distortion of the elements ahead of the crack front that normally occurs in cases where SBs are used, especially for complex model and crack geometry [28].

3. Results and discussion

3.1. Case study: results

The analytical results and the comparison between different approaches have been reported in Table 1.

3.2. FEM and DBEM analyses

Numerical models corresponding to the geometric model shown in Fig. 1 were created by means of a FEM-based and a DBEM-based software, respectively. Then, two commercial codes FEM and DBEM-based namely Abaqus [18] and Beasy [19], have been employed respectively to model the square plate of a unit thickness for both 2D and 3D cases. Later, the 45° tilted crack have been inserted in the square plate for both 2D and 3D cases. Moreover, the Young's modulus and the Poisson's ratio chosen to model the square plate have been placed equal to 206,000 MPa and 0.3, respectively. Then, boundary conditions have been applied to the numerical model for reproducing the case of a plate uniaxially loaded along the Y direction of the global reference system. Geometrical dimensions, loading and boundary conditions have been reported in Fig. 7 for the 2D Beasy model. These crack modelling techniques have been already extensively used in the past in several works [20–24,32]. Especially, the combination of the FEM-DBEM methods has proven the importance of this approach in the study of fatigue crack propagation [25,26].

3.2.1. DBEM analysis

A first evaluation of stress field and SIFs has been performed in a bi-

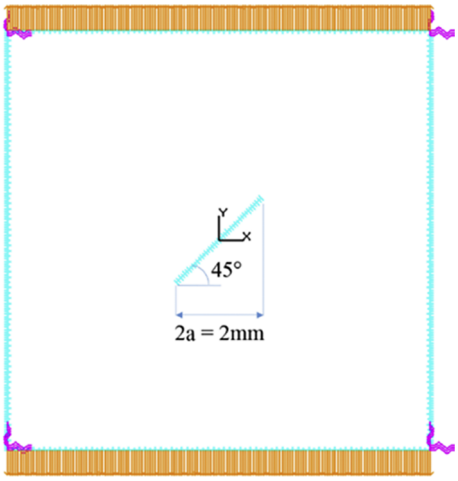

Fig. 7. Highlight of the mesh adopted for the square plate with the 45° tilted crack with boundary conditions.

dimensional environment using the DBEM code (Beasy) [19]. The square plate has been modelled with four lines subsequently meshed with quadratic elements. Later, an embedded crack tilted of an angle $\phi = 45^{\circ}$, compared to the X-axis, is inserted meshed in the center of the square plate. The projection of the tilted crack along the X-axis provides a crack length equal to 2a = 2 mm. Then, tractions equal to 1.0 MPa and −1.0 MPa and directed along the Y-axis have been applied on the upper and lower surfaces of the plate, respectively. Springs of stiffness equal to 10 N/mm have been introduced in the model as boundary conditions (Fig. 7) to eliminate the degrees of freedom of rigid body. The whole model has been meshed with 320 and 340 quadratic elements for the uncracked and cracked configurations, respectively.

For the cracked plate in the undeformed and deformed configurations, two plots of the stress field have been reported in Fig. 8(a and b), respectively.

In the 3D case, the numerical solution was carried out by means of a model with the same geometry of the 2D model and on which the same load and boundary conditions, used for solving the 2D problem (Fig. 9), have been applied. In this case, the thickness of the body, equal to 1 mm, was explicitly modelled. Hence, the adopted mesh was made of total 1913 quadratic elements with 42,015 nodes whilst, for the embedded crack only 104 quadratic elements have been used. The K_I and K_{II}, subsequently normalised, have been calculated using the most external J-path with a radius equal to 0.025 mm. Furthermore, a second DBEM analysis was carried out to obtain SIFs from a smaller J-path radius. In the latter case, the global mesh was made of 3042 quadratic elements and 66,285 nodes whilst, for the embedded crack, 212 quadratic elements with a J-path radius equal to 0.01 mm have been used. Then, the contour plots of the principal stress, $\sigma_{yy,}$ on deformed scale has been shown in Fig. 9 with highlight of the refined mesh on the crack fronts.

In Fig. 10 more details of the 3D crack, for the case with refined mesh, are shown.

3.2.2. *Three-dimensional FEM analysis*

Calculations of stresses and SIFs are carried out by means of the interaction between Abaqus, as FEM modeler and solver, and Zencrack as fracture mechanics tool [17]. This latter is necessary to insert the embedded crack and to evaluate the SIFs on the free surface or along the crack front. Hence, Zencrack generates a crack front starting from of a meshed uncracked model and substituting each original element, where the crack front will take place, with a unit block of cracked elements taken from a library where they are stored in form of families [17]. Each unit block differs from each other for the number of contained elements. To have more or less refined meshes on the crack front the user can select a cracked block with more or less elements, respectively. In this work, three kinds of unit blocks are employed to model the crack. The first is a SB belonging to the SB04 family, which provides the maximum accuracy for that family. The second and third are LBs belonging to LB02 and LB06 families, respectively, which provide the maximum accuracy for those families. Then, three analyses are carried out using three different approaches as shown in Figs. 12, 14 and 16. Furthermore, several J-paths with different radius are disposed along the crack fronts.

3.2.2.1. Standard blocks belonging to SB04 family. The FE model was meshed with SB04 that contains a total of 121,980 fully quadratic elements with 532,514 nodes. The K_I and K_{II} have been calculated in agreement of the third J-path (third ring), where the distance from the crack front is 0.002 mm (J-path radius). Similarly, to the DBEM model, nodal constraints have been applied on four nodes in the plane at half the thickness of the square plate, to remove the degrees of freedom of rigid body (Fig. 11). Hence, the principal stresses, $\sigma_{22,}$ have been plotted for the undeformed and deformed configurations, respectively

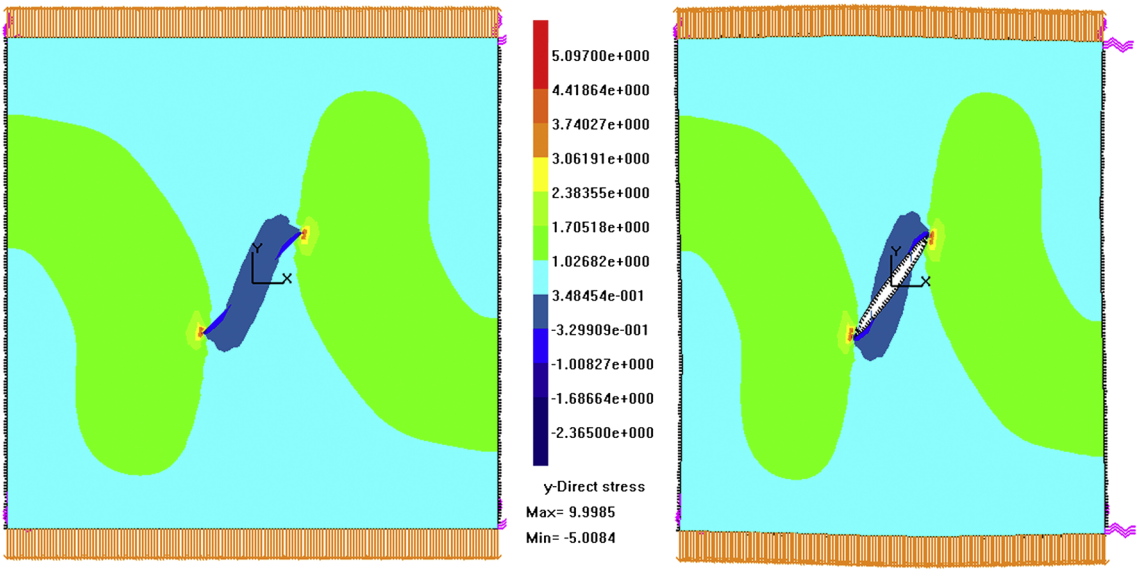

Fig. 8. Principal stresses σ_{22} on the undeformed plot (a) and on the deformed plot (b).

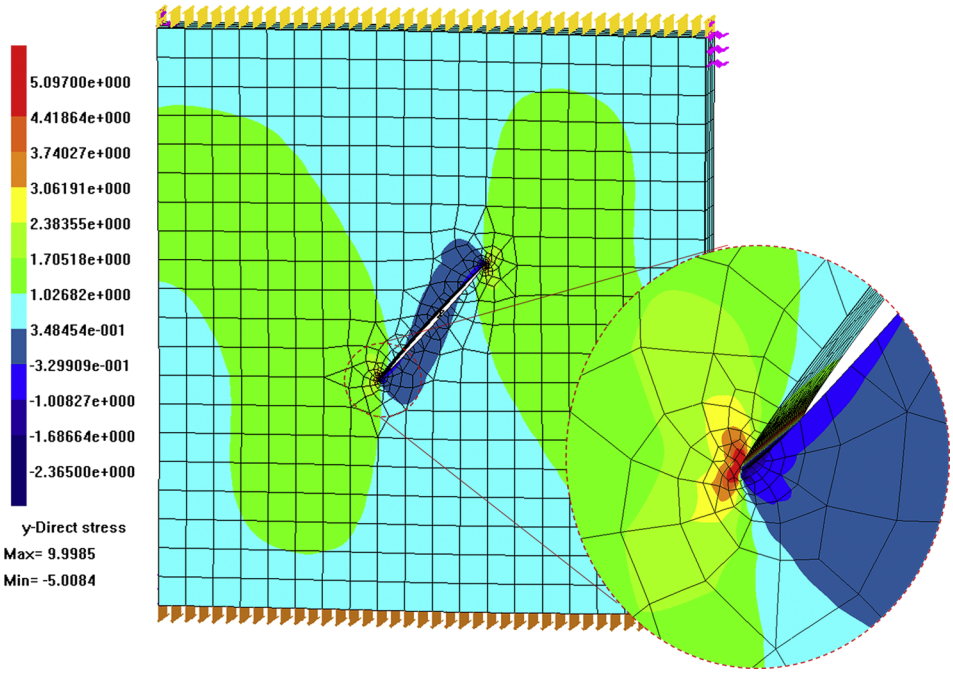

Fig. 9. Contour plot of principal stresses, σ_{yy}, on deformed plot with highlight of the crack front.

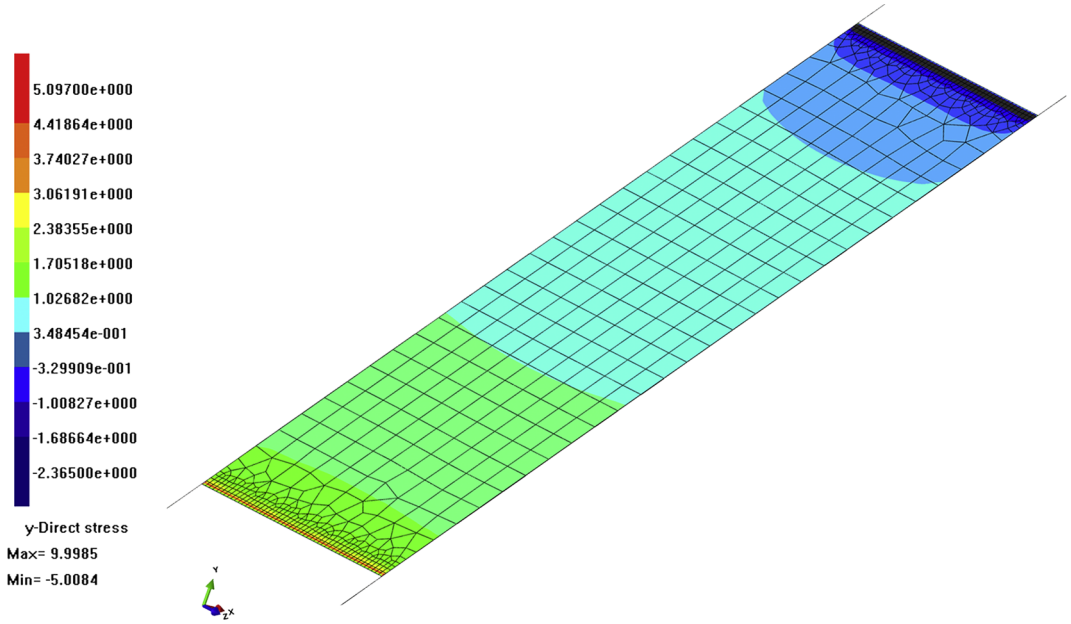

Fig. 10. Contour plot of σ_{yy} with highlight of a crack front.

(Fig. 11). The maximum value of the stress scale was the same adopted for the corresponding DBEM analysis whilst, the minimum scale value was set to −1 MPa to better evidence the stress field in the plate. However, the stress distribution is substantially the same previously calculated in the DBEM analysis and the symmetry of the square plate permits to consider only the SIFs calculated on a crack front.

In Fig. 12, the previous stress scenario has been shown for the 45° cut model to highlight the surface containing the two crack fronts. J-paths have been highlighted for only one crack front.

3.2.2.2. Large blocks belonging to LB02 family. In this case, a hexagonal volume containing the tilted crack has been meshed with LBs of family LB02. The model was meshed with a total of 123,024 fully quadratic elements with 537,704 nodes. The K_I and K_{II} have been calculated in agreement of the second ring (second J-path) where the distance from the crack front was equal to 0.1 mm (J-path radius). In Figs. 13 and 14, the principal stress field, $\sigma_{22,}$ has been shown with highlight of a crack front on the deformed plot. Moreover, the mesh on the cracked surfaces has been highlighted as well as the j-paths along the crack front (Fig. 14).

3.2.2.3. Large blocks belonging to LB06 family. This model contains a hexagonal volume meshed with LBs of family LB06. In this case, the model has been meshed with a total 134,288 fully quadratic elements with 586,952 nodes. The K_I and K_{II} have been calculated in agreement of the second ring where the distance from the crack front is equal to 0.1 mm (J-path radius). The part 1 of this model is meshed with the same number of quadrilateral elements as in the previous case whilst, to

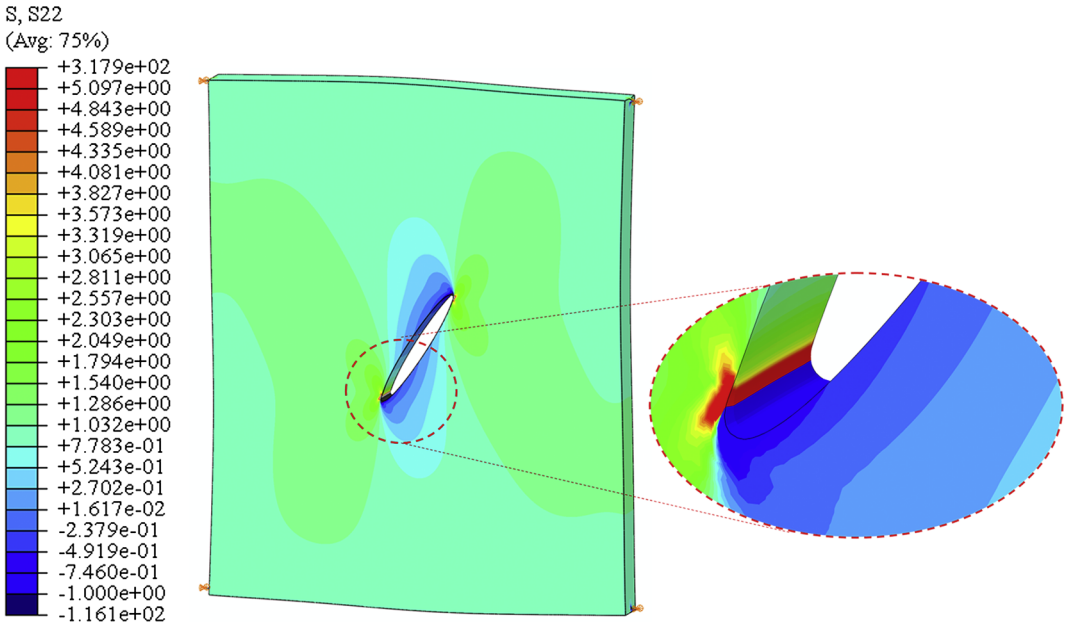

Fig. 11. Contour plots of the principal stresses, σ_{22}, for the undeformed and deformed configurations, respectively, with highlight of the stress scenario for a single cracked zone.

model the crack, the part 2 is meshed by using LBs more enriched of elements and belonging to family LB06. Also, in this case the principal stress, σ_{22}, and some details of the crack front as well as the j-paths have been highlighted. Comparing Figs. 13,14 and 15,16, respectively, it is worth noting that the stress field slightly changes. The stress scenario reported in Figs. 15 and 16 shows a more accurate evaluation of the stress field because a greater number of elements has been used for modelling the crack. Therefore, the result of the latter analysis can be considered as the convergence result. The same occurs for the SIFs values.

3.2.2.4. Comparison of normalised SIFs. The SIFs, K_I and K_{II}, obtained from the numerical analyses and distributed along the crack front have been reported in normalised form in Figs. 17 and 18. Hence, in Table 2, all the calculated values of the K_1 and K_2, related to the analytical and numerical analyses, have been reported. Similarly, in Table 3, the K_1 and K_2 values, calculated at the intersection of the crack front with the free surface, have been reported. Then, the K_1 and K_2 values calculated at the midside position of the crack front have been shown in Table 4.

Each cracked block of family LB06 has about 86,000 quadrilateral elements while each cracked block of family LB02 holds about 63,500 quadrilateral elements. Moreover, each cracked block of family SB04 holds only 35 quadrilateral elements. Hence, the LB06 can have up to 8 contours for j-integral calculation, the LB02 can have up to 12 contours for J-integral calculation while the SB04 can have up to 6 contours for j-integral calculation. Despite the different peculiarities of each cracked block, in this case the three different families of cracked blocks have been used only to study the convergence of results because they allow to mesh the crack with a very different number of elements.

In Figs. 17 and 18 the normalised K_I (K_1) and normalised K_{II} (K_2), obtained from the numerical FEM and DBEM-based analyses versus the dimensionless length of the crack fronts have been reported. The trends

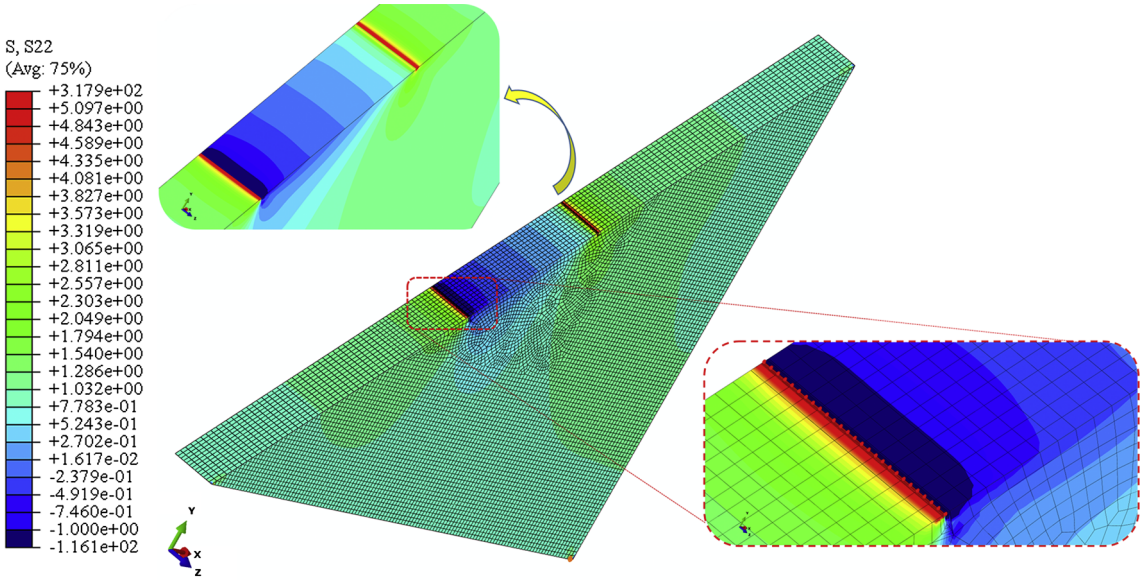

Fig. 12. Contour plot of the principal stress, σ_{22}, for the 45° cut square plate with highlight of the J-paths along a crack front.

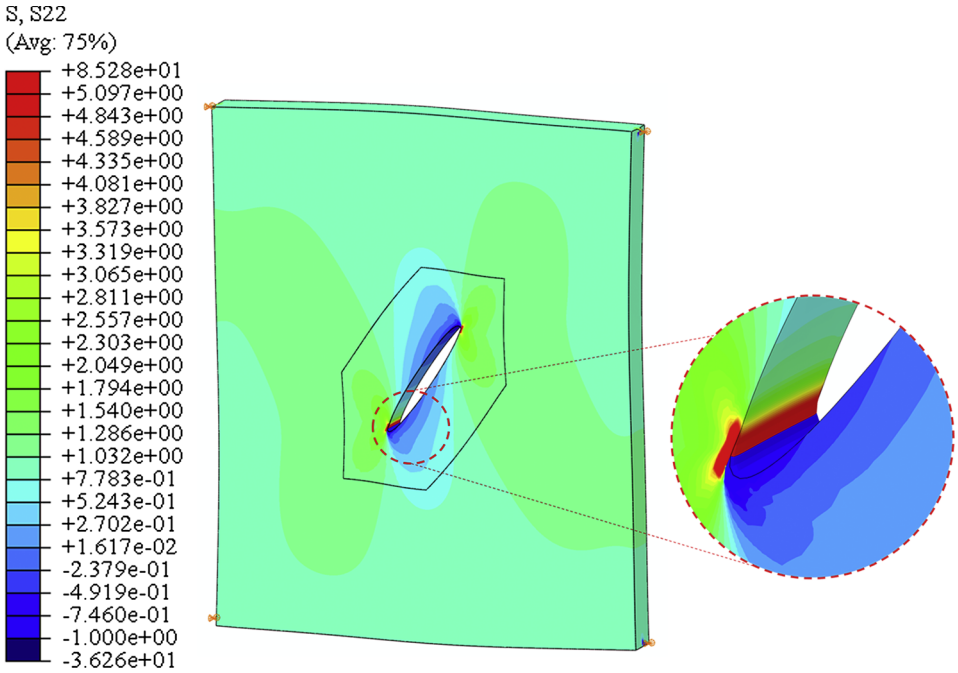

Fig. 13. Contour plots of the principal stress, σ_{22}, for the undeformed and deformed configurations, respectively, with highlight of the stress scenario for a single cracked zone.

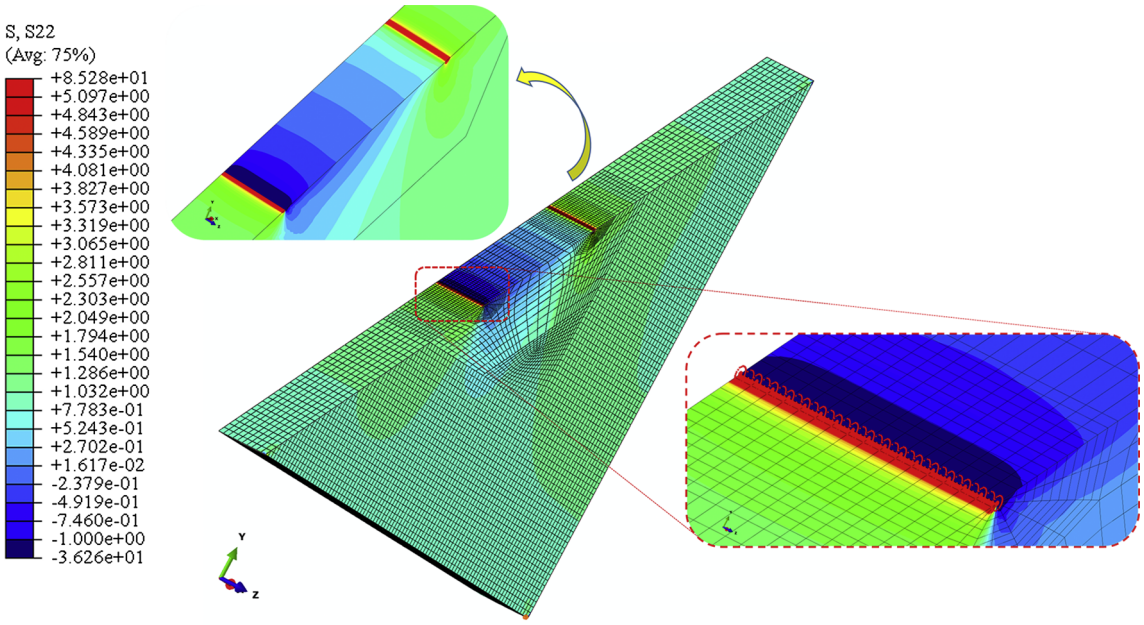

Fig. 14. Contour plot of the principal stress, σ_{22}, for the 45° cut square plate with highlight of J-paths along the crack front.

of different K_1 show a good agreement along the crack front except for that values calculated on the free surfaces, where they converge in pairs. Hence, the K_1 produced by DBEM and FEM-based (SB04) analyses converge to the same value (0.61 MPa) whilst the second pairs, that have been produced by the two FEM-based analyses (with LB06 and LB02) converge to the value of 0.64 MPa. The trends of the K_2 values, obtained from the FEM-based analyses, show a good agreement along the whole crack front and then in correspondence of the intersection between the crack front and the free surfaces. On the other hand, the K_2 values, obtained from the DBEM-based analysis, show a good agreement in correspondence of the breakthrough points but not along the whole crack front, where the maximum percentage difference located at the midside position is equal to 7.1%.

3.2.2.5. Thickness effect on normalised SIFs. A study to evaluate the effect produced by the increasing of the thickness on normalized SIFs has been also carried out. Starting from a square plate of unit thickness, four increments in the thickness, each one equal to 0.5 mm, have been assessed. In Tables 3 And 4, results of these calculations have been reported whilst, in Figs. 19, 20 and Figs. 21, 22, a comparison among these results have been shown in more details. These results have been evaluated both where the crack front intersects the free surfaces of the plate and at the deepest point of the crack front. In this case, all the FEM and DBEM-based numerical analyses have been carried out considering only 3D models with elements distribution on the external surfaces as for the previous cases, except for the distribution of elements along the thickness direction that has been changed.

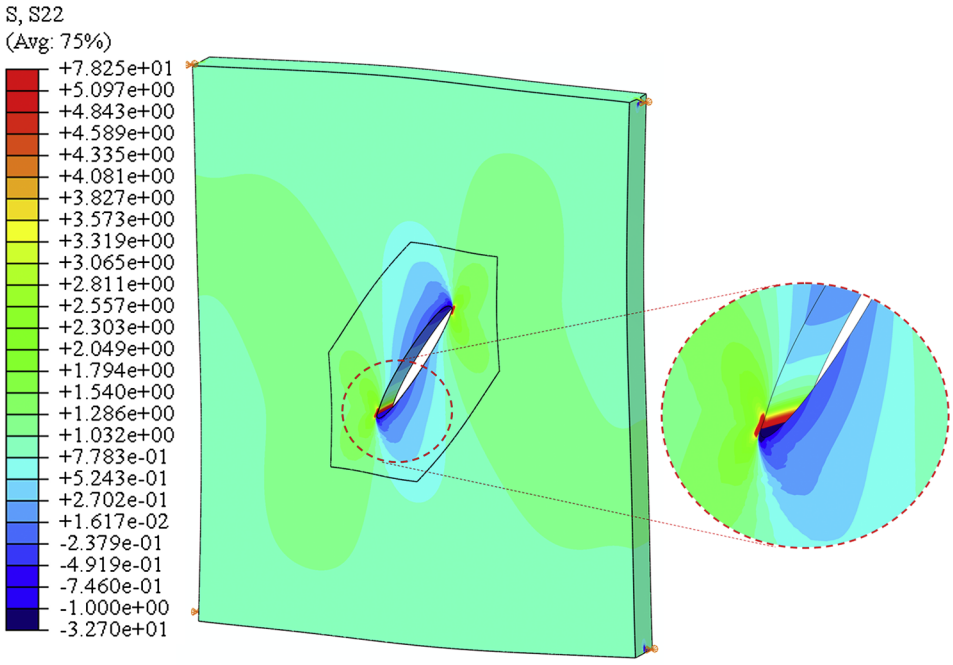

Fig. 15. Contour plots of principal stress, σ_{22}, for the undeformed and deformed configurations, respectively, with highlight of the stress scenario for a single cracked area.

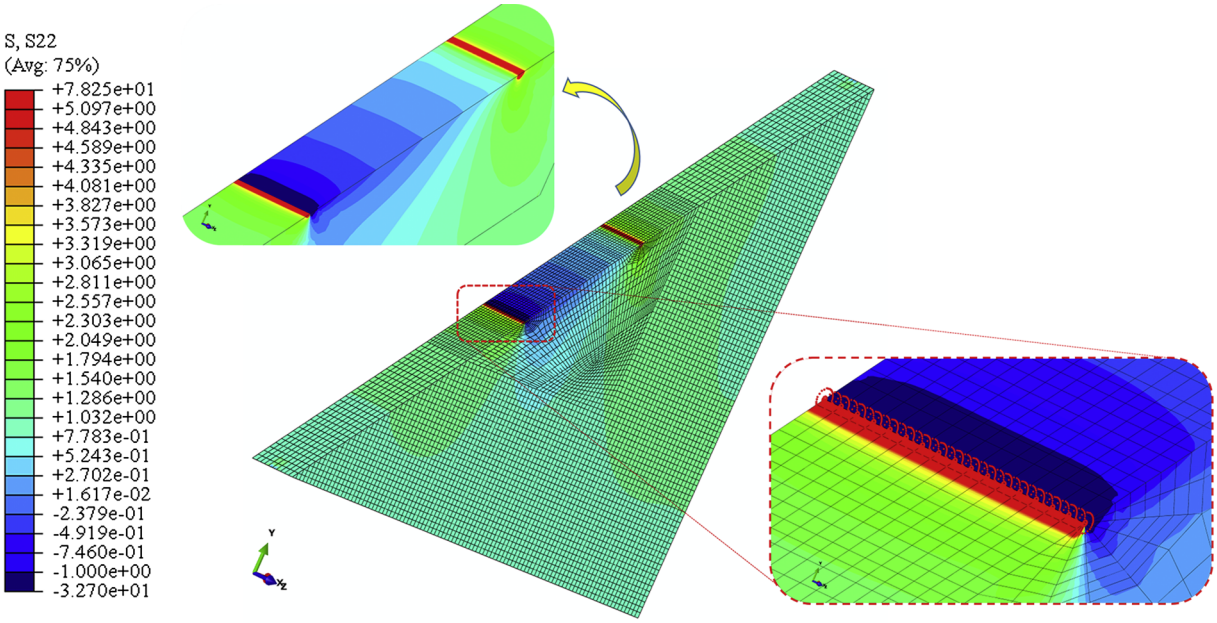

Fig. 16. Contour plot of principal stress, σ_{22}, for the 45° cut square plate with highlight of J-paths along the crack front.

From Fig. 19, it is worth noting that normalised K_I, obtained from the FEM-based analyses that use LBs of family LB02 and LB06 are quite insensitive as the thickness increases. Moreover, the maximum percentage difference between the starting values for t = 1.0 mm and assessed on the free surface is equal to 0.62%. The explanation is that, within the LB, the mesh is distributed in such a way that the rings constructed for the J-contour calculation allow to obtain more accurate SIF than those obtained with the use of SB. Hence, percentage differences are greater if SBs have been used in the FE analysis. In the latter case the maximum difference for t = 1.0 mm was equal to 5.6%. On the other hand, the DBEM based solution provides an intermediate value of normalised K_I showing a maximum percentage difference, with respect to the corresponding FEM based analysis with LB06, equal to 4%. It is worth noting that, all the normalised K_I values tend to decrease as the thickness increases up to 2.0 mm, after that normalised K_I values tend to increase as the thickness increases up to the final value equal to 3.0 mm.

On the other hand, observing the results shown in Fig. 20, it is worth noting that trend of K_2 values obtained from the FEM-based analyses by using of LB02 and LB06 change as the thickness increases. Moreover, the maximum percentage difference between the starting values of K_2 (t = 1.0 mm) and evaluated on the free surfaces of the plate is equal to 0.5%. As in the previous case for t = 1.0 mm, the percentage differences are greater if in the FE analysis SBs have been used. In the latter case, the maximum percentage difference calculated for t = 1.0 mm is equal to 5.5%. The DBEM based solution returns intermediate value of K_2 with respect to the FEM-based solution by using LB02 and LB06,

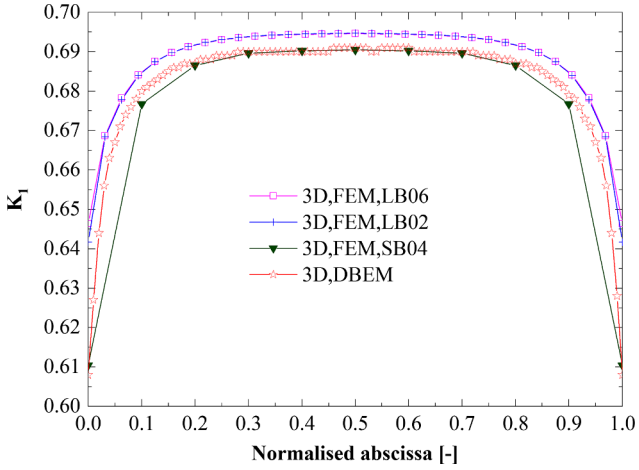

Fig. 17. 3D Beasy and Zencrack normalised K_I comparison.

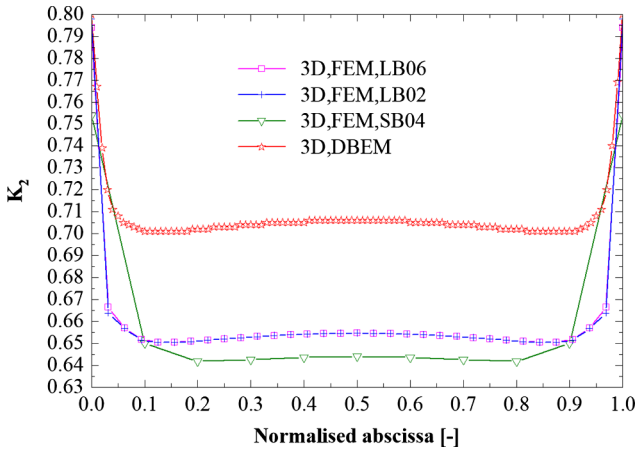

Fig. 18. 3D Beasy and Zencrack normalized K_2 comparison.

showing a maximum percentage difference equal to 2.4% for t = 1.0 mm. It is interesting to observe that K_2 values, related to the case where LBs have been used, tend to decrease as the thickness increases up to the final value equal to 3.0 mm. On the contrary, the K_2 values obtained from the FEM based analysis, in which SBs have been used, and the K_2 values obtained from the DBEM-based solution tend to increase as the thickness increases until the value of 2.0 mm, respectively. Furthermore, the K_2 values tend to decrease as the thickness increases until the final thickness (3.0 mm) has been reached. In the latter case, a convergence value of K_2 can be obtained considering a comparison between the FEM-DBEM based solutions that corresponds to about 0.773 MPa (Table 3).

The K_1 obtained from the FEM-based analyses that use LB02, LB06 or SB04, and the corresponding K_1 values, obtained from the DBEM based analyses, have been all evaluated at midside position of the crack

Table 4
Comparison among the normalised SIFs calculated by 3D FEM and DBEM-based numerical analyses at the midside position of the crack front.

	SB04 Midside position R = 0.002		LB02 Midside position R = 0.1		LB06 Midside position R = 0.1		Beasy Midside position R = 0.1	
Thickness	K_1	K_2	K_1	K_2	K_1	K_2	K_1	K_2
1.0	0.690	0.644	0.695	0.655	0.695	0.655	0.690	0.705
1.5	0.686	0.645	0.690	0.655	0.690	0.655	0.687	0.708
2.0	0.682	0.646	0.686	0.657	0.686	0.657	0.683	0.709
2.5	0.678	0.646	0.682	0.658	0.682	0.657	0.679	0.711
3.0	0.674	0.645	0.678	0.658	0.678	0.658	0.676	0.711

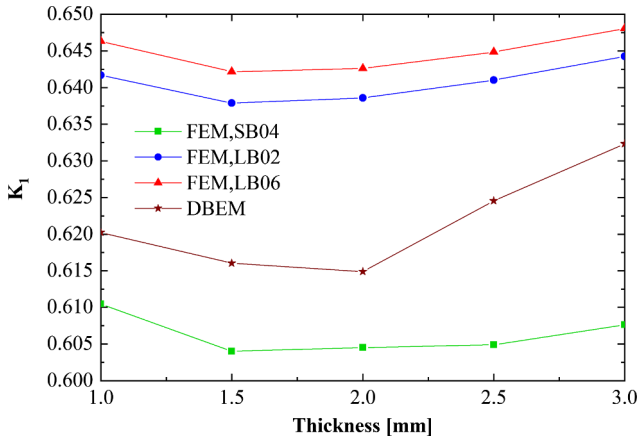

Fig. 19. Comparison of the normalized K_I at free surface and with increasing thickness.

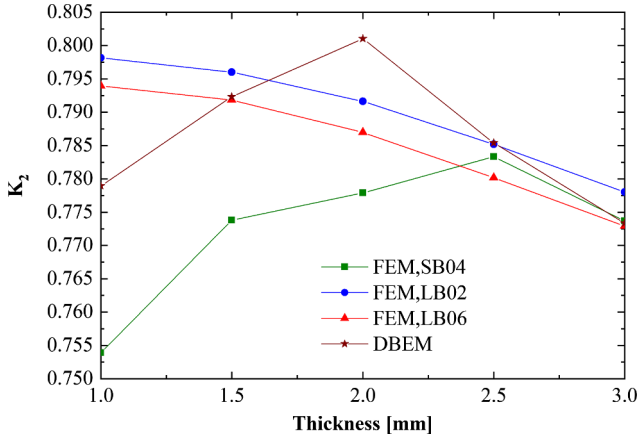

Fig. 20. Comparison between the K_2 values, obtained from the FEM-DBEM based analyses, calculated at the free surfaces and with increasing thickness.

Table 3
Comparison among the normalised SIFs calculated by 3D numerical analyses (FEM, DBEM) on the free surface.

	SB04 Free surface R = 0.002		LB02 Free surface R = 0.1		LB06 Free surface R = 0.1		Beasy Free surface R = 0.1	
Thickness	K_1	K_2	K_1	K_2	K_1	K_2	K_1	K_2
1.0	0.610	0.754	0.642	0.798	0.646	0.794	0.620	0.779
1.5	0.604	0.774	0.638	0.796	0.642	0.792	0.616	0.792
2.0	0.605	0.778	0.639	0.792	0.643	0.787	0.615	0.801
2.5	0.605	0.783	0.641	0.785	0.645	0.780	0.625	0.785
3.0	0.608	0.774	0.644	0.778	0.648	0.773	0.632	0.773

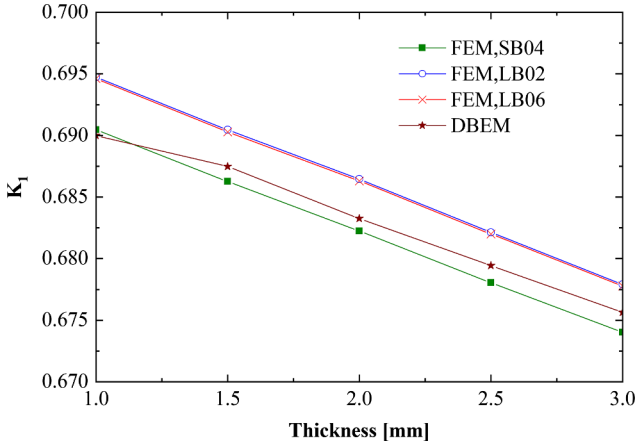

Fig. 21. Comparison of the K_1 values calculated at midside position of the crack front and with increasing thickness.

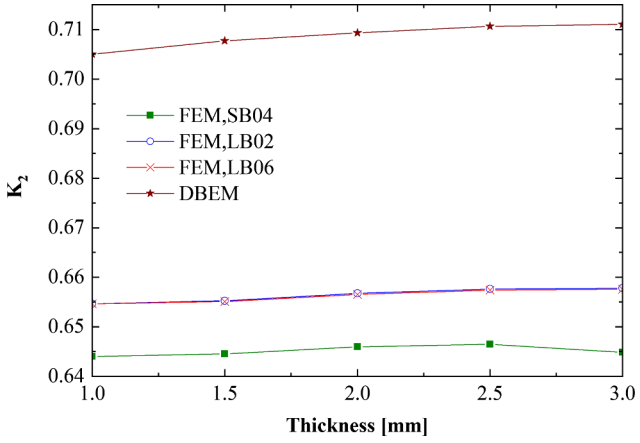

Fig. 22. Comparison of the K_2 calculated at midside position of the crack front and with increasing thickness.

front and have been shown in Fig. 21. It is worth noting that, K_1 values change as the thickness increases. In this case, the maximum difference among all the calculated K_1 values for t = 1.0 mm is equal to 0.72%. Hence, the DBEM based solution returns intermediate values of the K_1, calculated along the crack front, up to the final thickness (3.0 mm). It is interesting to observe that, all the K_1 values tend to decrease as the thickness increases, namely from the initial thickness (1.0 mm) to the final thickness (3.0 mm). However, these results have shown a certain insensitivity to the variation of K_1 as the thickness increases.

On the other hand, observing Fig. 22, it is worth noting that K_2 values obtained from the FEM-based analyses that use LB02 and LB06, respectively, substantially do not change with increasing of thickness. Moreover, the maximum percentage difference between the K_2 values for t = 1.0 mm is equal to 0.5%. As for the previous case, the percentage differences have been greater if in the FE analyses SBs have been used. Then, in the latter case, the maximum percentage difference evaluable, compared to the case in which LB06 have been used, is equal to 1.7% for t = 1.0 mm. The DBEM-based solution returns the highest value of the K_2 showing a maximum percentage difference, compared to the K_2 values obtained from a FEM based analysis with LB06, which is equal to 7.1%. It is worth noting that K_2 values, related to the case where SBs have been used, tend not to change as the thickness increases. On the contrary, the K_2 values obtained from the DBEM-based solution tend to increase slightly as the thickness increases.

4. Conclusions

Results shown in Tables 1 and 2 have been obtained for a notched plate subjected to mixed mode I + II loading, by adopting coarse meshes if the approximate methods for rapid calculation of NSIFs have been used. Conversely, finer meshes have been used considering Gross and Mendelson's equations as well as for both FEM and DBEM-based numerical simulations. It is worth noting that the percentage error has been found about 12% for the case of tilted cracks with Treifi and Oyadiji approach (Table 1). For the method based on the evaluation of total and deviatoric SED, a percentage error, close to that observed in the case of Treifi and Oyadiji, has been found. However, the deviation remains greater than that observed in the case of Lazzarin et al., because of the dependence of the deviatoric SED on the mesh size. This problem has been overcome by the modified version of the method based on deviatoric SED that, through a control volume consisting of a circular ring, has enabled to exclude the region characterized by the highest stress gradient making the method less sensitive to the refinement level of the adopted mesh. The method based on deviatoric SED, and in particular the modified version, has provided very good approximations and a greater applicability than the approach of Lazzarin et al. so it could be useful for rapid calculation of the NSIFs. Furthermore, two different numerical analyses have been carried out by using commercial software based on FEM and DBEM, respectively. The NSIFs have been firstly calculated at the intersection between the crack front and the free surface of the part under investigation. Then, a good level of agreement among the K_1 and K_2 (NSIFs), calculated analytically by the methods for rapid calculation of NSIFs and those calculated by FEM and DBEM-based numerical analyses, has been found. Secondly, the effect produced on NSIFs according to the increasing thickness has been performed. Hence, starting from the unit thickness, four steps with increments of 0.5 mm each one, have been considered and the solutions for the K_1 and K_2 have been reported. The K_1 have shown greater sensitivity with increasing thickness, whilst the K_2 have not shown significant variations with increasing thickness.

References

[1] A. Seweryn, Brittle fracture criterion for structures with sharp notches, Eng. Fract. Mech. 47 (5) (1994) 673–681.
[2] T. Boukharouba, T. Tamine, L. Niu, C. Chehimi, G. Pluvinage, The use of notch stress intensity factor as a fatigue crack initiation parameter, Eng. Fract. Mech. 52 (3) (1995) 503–512.
[3] B. Atzori, G. Meneghetti, Fatigue strength of fillet welded structural steels: finite elements, strain gauges and reality, Int. J. Fatigue 23 (8) (2001) 713–721.
[4] P. Lazzarin, R. Tovo, A notch intensity factor approach to the stress analysis of welds, Fatigue Fract. Eng. Mater. Struct. 21 (9) (1998) 1089–1103.
[5] P. Lazzarin, R. Zambardi, A finite-volume-energy based approach to predict the static and fatigue behavior of components with sharp V-shaped notches, Int. J. Fract. 112 (3) (2001) 275–298.
[6] P. Livieri, P. Lazzarin, Fatigue strength of steel and aluminium welded joints based on generalised stress intensity factors and local strain energy values, Int. J. Fract. 133 (3) (2005) 247–276.
[7] M. Treifi, S.O. Oyadiji, Strain energy approach to compute stress intensity factors for isotropic homogeneous and bi-material V-notches, Int. J. Solids Struct. 50 (14–15) (2013) 2196–2212.
[8] P. Lazzarin, F. Berto, M. Zappalorto, Rapid calculations of notch stress intensity factors based on averaged strain energy density from coarse meshes: theoretical bases and applications, Int. J. Fatigue 32 (10) (2010) 1559–1567.
[9] B. Gross, A. Mendelson, Plane elastostatic analysis of V-notched plates, Int. J. Fract.Mech. 8 (3) (1972) 267–276.
[10] M.L. Williams, Stress singularities resulting from various boundary conditions in angular corners on plates in extension, J. Appl. Mech. 19 (1959) 526–528.
[11] A. Campagnolo, F. Berto, P. Lazzarin, The effects of different boundary conditions on three-dimensional cracked discs under anti-plane loading, Eur. J. Mech. – A/Solids 50 (2015) 77–86.
[12] F. Berto, P. Lazzarin, Recent developments in brittle and quasi-brittle failure assessment of engineering materials by means of local approaches, Mater. Sci. Eng. R 75 (1) (2014) 1–48.
[13] F. Berto, A. Campagnolo, P. Gallo, Brittle failure of graphite weakened by V-notches: a review of some recent results under different loading modes, Stren. Mater. 47 (3) (2015) 488–506.
[14] A. Campagnolo, F. Berto, D. Leguillon, Fracture assessment of sharp V-notched components under Mode II loading: a comparison among some recent criteria,

Theor. Appl. Fract. Mech. (2016), https://doi.org/10.1016/j.tafmec.2016.02.001.
[15] A.R. Torabi, A. Campagnolo, F. Berto, Tensile fracture analysis of V-notches with end holes by means of the local energy, Phys. Mesomech. 18 (3) (2015) 194–202.
[16] F. Berto, A. Campagnolo, F. Chebat, M. Cincera, M. Santini, Fatigue strength of steel rollers with failure occurring at the weld root based on the local strain energy values: modelling and fatigue assessment, Int. J. Fatigue 82 (2016) 643–657.
[17] Zencrack v8.2.2 - 12,2017, Documentation, Zentech International Limited, 2017.
[18] Dassault Systems, Simulia Corp 2011, Abaqus analysis user's manual, Version 6.12. 1, Providence, RI, USA.
[19] BEASY 2016, BEASY V10r18 Documentation, C.M. BEASY Ltd.
[20] M. Lepore, P. Carlone, F. Berto, R. Sonne Mads, A FEM based methodology to simulate multiple crack propagation in friction stir welds, Eng. Fract. Mech. 184 (2017) 154–167, https://doi.org/10.1016/j.engfracmech.2017.08.024.
[21] R. Citarella, P. Carlone, R. Sepe, M. Lepore, DBEM crack propagation in friction stir welded aluminum joints, Adv. Eng. Softw. 101 (2016) 50–59.
[22] M. Lepore, F. Berto, On the fatigue propagation of multiple cracks in friction stir weldments using linear and non-linear models under cyclic tensile loading, Eng. Fract. Mech. 206 (2019) 463–484.
[23] R. Citarella, M.A. Lepore, A. Maligno, V. Shlyannikov, FEM simulation of a crack propagation in a round bar under combined tension and torsion fatigue loading, Fatica ed Integrità Strutturale 9 (2015) 97–119.
[24] R. Citarella, M. Lepore, V. Shlyannikov, R. Yarullin, Fatigue surface crack growth in cylindrical specimen under combined loading, Eng. Fract. Mech. 131 (2014) 439–453.
[25] R. Citarella, P. Carlone, M. Lepore, G.S. Palazzo, A FEM-DBEM investigation of the influence of process parameters on crack growth in aluminum friction stir welded butt joints, Int. J. Mater. Form. 8 (4) (2015) 591–599.
[26] R. Citarella, P. Carlone, R. Sepe, M. Lepore, Hybrid technique to assess the fatigue performance of multiple cracked FSW joints, Eng. Fract. Mech. 162 (2016) 38–50.
[27] L. Pittarello, A. Campagnolo, F. Berto, NSIFs estimation based on the averaged strain energy density under in-plane mixed mode loading, Proc. Struct. Integ. 2 (2016) 1829–1836.
[28] R. Citarella, V. Giannella, M. Lepore, G. Dhondt, Dual boundary element method and finite element method for mixed-mode crack propagation simulations in a cracked hollow shaft, Fatigue Fract. Eng. Mater. Struct. 41 (2018) 84–98.
[29] P. Lazzarin, A. Campagnolo, F. Berto, A comparison among some recent energy- and stress-based criteria for the fracture assessment of sharp V-notched components under Mode I loading, Theor. Appl. Fract. Mech. 71 (2014) 21–30.
[30] D. Leguillon, A criterion for crack nucleation at a notch in homogeneous materials, Comptes Rendus de l'Acadèmie des Sciences – Series IIB – Mechanics 329 (2001) 97–102.
[31] A. Carpinteri, P. Cornetti, N. Pugno, A. Sapora, D. Taylor, A finite fracture mechanics approach to structures with sharp V-notches, Eng. Fract. Mech. 75 (2008) 1736–1752.
[32] M. Lepore, F. Berto, D. Kujawski, Non-linear models for assessing the fatigue crack behaviour under cyclic biaxial loading in a cruciform specimen, Theor. Appl. Fract. Mech. 100 (2019) 14–26.